M3LW-16OR0402153
PNNL-25854

Light Water Reactor Sustainability Program

Mechanical Properties of 304L and 316L Austenitic Stainless Steels after Thermal Aging for 1500 Hours

Cast Stainless Steel Aging (LW-16OR040215)

September 2016

U.S. Depart of Energy

Office of Nuclear Energy

M3LW-16OR0402153
PNNL-25854

Department of Energy/Office of Nuclear Energy

LWR Sustainability R&D

Cast Stainless Steels Aging (WP#: LW-16OR040215)

Mechanical Properties of 304L and 316L Austenitic Stainless Steels after Thermal Aging for 1500 Hours

by

Thak Sang Byun

Timothy G. Lach

Pacific Northwest National Laboratory

operated by

Battelle

for the

U.S. Department of Energy

under contract DE-AC05-76RL01830

Contents

LIST OF TABLES AND FIGURES

MECHANICAL PROPERTIES OF 304L AND 316L AUSTENITIC STAINLESS STEELS AFTER THERMAL AGING FOR 1500 HOURS

T.S. Byun and T.G. Lach
Nuclear Sciences Division, Pacific Northwest National Laboratory, Richland, WA 99352

1. EXECUTIVE SUMMARY

This report presents the mechanical test data of 304L and 316L austenitic stainless steels before and after thermal aging for 1500 hours. These alloys were selected as reference materials for comparison with the case austenitic stainless steels (CASSs). The aging degradation of CASS components is an important concern in the extended operation of light water reactors (LWRs) not only because the aging phenomena beyond the reactor operating experiences are not fully understood, but also because replacement of such massive components would be prohibitively expensive [1,2]. The ongoing research, Cast Stainless Steel Aging, aims to expand scientific understanding on thermal-aging induced degradation phenomena, and ultimately, to provide knowledge-based conclusive prediction for the integrity of the CASS components of LWR power plants during the service life extended up to and beyond 60 years [3].

Most CASS materials used in nuclear power plants have a duplex structure of austenitic (γ) matrix and 3–40% ferritic (δ) phase. It is known that any cast microstructure containing a significant amount (>20%) of δ-ferrite can become susceptible to the thermally-induced embrittlement in the reactor operating temperature range 280–340 °C [1-6]. The primary brittle fracture mechanism observed in a thermally embrittled duplex stainless steel is cleavage initiation at ferrite followed by propagation through separation of ferrite-austenite phase boundary, and such cracking mechanism could be caused or enhanced by various microstructural changes during thermal aging, such as formation of a Cr–rich α'-phase through the spinodal decomposition of δ-ferrite, precipitation of G-phase and $M_{23}C_6$ carbide, and additional precipitation and growth of carbides and nitrides at ferrite-austenite phase boundaries [4-21]. It is known, however, that the precipitation of Cr–rich α'-phase in δ-ferrite is the main embrittlement mechanism in the cast stainless steels, while the thermal aging induces various precipitations in the austenite matrix but usually causes a negligible to moderate effect on the properties of the phase [6-9]. These observations naturally lead to a prediction that the pure austenitic stainless steels with similar chemistries as those of CASS alloys will not experience thermal embrittlement in comparable time periods.

To obtain the reference data and compare with the thermally-induced changes in the cast austenitic stainless steels, two fully austenitic alloys (i.e., type 304L and 316L alloys) have been aged at 290–400°C for 1500 hours and characterized. This report will describe the mechanical property changes in 304L and 316L austenitic stainless steels due to the shortest term (1500 h) thermal aging. In this report the uniaxial tensile test and Charpy impact test data comprise the key datasets used to discuss the effects of thermal aging. To obtain the tensile property data in each alloy and aging condition, seven SS-3 specimens with a gage section of 7.62×0.76×1.52 mm were tested at a displacement rate of 0.5 mm/min and at RT, 100, 200, 290, 330, 360, and 400 °C, respectively. In the Charpy impact testing, meanwhile, twelve standard sized specimens,

i.e., V-notched bars of 10×10×55 mm, were tested at selected 12 temperatures ranging from liquid nitrogen temperature to 300 °C. Each dataset with twelve absorbed energy values was analyzed using the standard regression method based on the hyperbolic tangent function to determine the parameters such as the ductile-brittle transition temperature (DBTT) and upper shelf energy (USE). It is shown that no noticeable degradation is observed in both the tensile property and the impact property after the 1500 hour aging. This result is highly contrasted with the cast stainless steels that have similar chemistries but show significant degradation in impact energy and tensile ductility (see the earlier report-M2LW-16OR0402152 for comparison).

2. EXPERIMENTAL

2.1. Test materials–two reference austenitic stainless steels

Two commercial austenitic stainless steels (type 304L and 316L alloys) in typical solution-annealed condition have been characterized before and after thermal aging. These alloys were chosen as reference materials for the CASS alloys studied in the project (i.e., CF3, CF3M, CF8, and CF8M) since their compositions are within the range of specifications for the cast alloys while their ferrite contents are negligible if any. Listed in Table 1 are the chemistry data obtained for the two reference alloys. These stainless steels were aged in the form of billet with a dimension of 31 × 38 × 250 mm at 290, 330, 360, and 400 °C for 1500 h.

Table 1. Chemistries of model cast austenitic stainless steels in wt.%

Grade*	Fe	Cr	Ni	Mn	Mo	Si	P	C	S	N
304L	Bal.	18.04	8.07	1.78		0.4	0.04	0.019	0.001	0.099
316L	Bal.	16.70	10.15	0.63	2.03	0.53	0.027	0.002	0.003	0.047

**In solution annealed condition (~1050 °C)*

2.2. Tensile and Charpy impact testing

To measure thermal aging effect on the strength and ductility of the two fully austenitic alloys, tensile tests were carried out at room temperature (RT) to 400°C for the alloys aged at 290, 330, 360, and 400 °C for 1500 hours. The tensile specimens were SS-3 dog-bone shaped flat specimens with the gage section dimensions of 7.62 mm in length × 0.76 mm in thickness × 1.52 mm in width, and were tested at a displacement rate of 0.5 mm/min at seven representative temperatures (i.e., RT, 100, 200, 290, 330, 360, and 400°C).

The standard Charpy test was also carried out for the two reference materials in aged and non-aged conditions. For each aging condition, an impact (or absorbed) energy versus temperature curve were obtained from the standard Charpy specimens (10 mm × 10 mm × 25 mm bend bar with a 2 mm deep 45° notch) in a temperature range of liquid nitrogen temperature to 300 °C. Impact tests were performed in a standard size Tinius-Olsen Charpy impact tester. For each materials condition, 12 tests were performed to construct a temperature transition curve.

Curve fitting analysis for the impact energy datasets was performed to obtain the temperature transition parameters using a four parameter hyperbolic tangent function [22, 23]:

$$E(T) = A + B \times \tanh\left(\frac{T-D}{C}\right) \qquad (eq.1)$$

where *A* is the vertical position of the inflection point, *B* is the vertical distance between point *A* and the upper and lower shelves, *C* is one-half the width of the transition region, and *D* is the horizontal position of the inflection point. Key transition curve parameters can be defined using these parameters: the value *A+B* is defined as the upper shelf energy (USE), and *A-B* is defined as the lower shelf energy (LSE). The parameter *D* becomes the ductile-brittle transition temperature (DBTT), which is the midpoint temperature in the temperature-transition region. In practical analysis the two parameters, the LSE and USE, can be determined by plotting measured absorbed energy data, and therefore the DBTT value is used as an iteration parameter. The LSE can be set at 20 J for both stainless steels [24].

3. TENSILE PROPERTIES AFTER 1500 H AGING

3.1. Thermal aging effect on strength

Figures 1 and 2 display the yield strength (YS) and ultimate tensile strength (UTS) of 304L and 316L stainless steels before and after thermal aging for 1500 hours. First of all, the strength versus temperature plots show that both YS and UTS decrease with test temperature up to 290 °C and experience little change over the aging temperature range of 290–400 °C. A simple comparison of the strength versus temperature plots indicates that the short-term thermal aging has not caused any significant change in the test-temperature dependence for both alloys. This may also indicate that the work-hardening mechanisms being operated in tension testing in the given test-temperature range remain unchanged after the short-term aging.

It is also recognized that neither age hardening nor age softening is apparent in both YS and UTS datasets. Each data cluster at a given temperature is contained within a narrow range; the band widths of the YS and UTS for each alloy are only 90–150 MPa. In detail, however, there are a few datasets that are consistently higher or lower within a limited temperature range: the UTS data for 304L alloy after aging 400 °C are on the top of the band over a temperature range of 100–360 °C and the 316L alloy aged at 330 °C has the lowest strength among the stainless steels in different conditions at several test temperatures. These can be vague evidences of, respectively, age hardening and softening. Overall, however, the variation of strength due to different aging conditions and alloys are within the scatter ranges of respective datasets. This strength behavior without apparent dependence on aging temperature should indicate that the strength change by the 1500 hour thermal aging at 290–400 °C is negligible or the hardening and softening components in the strength change are complement each other.

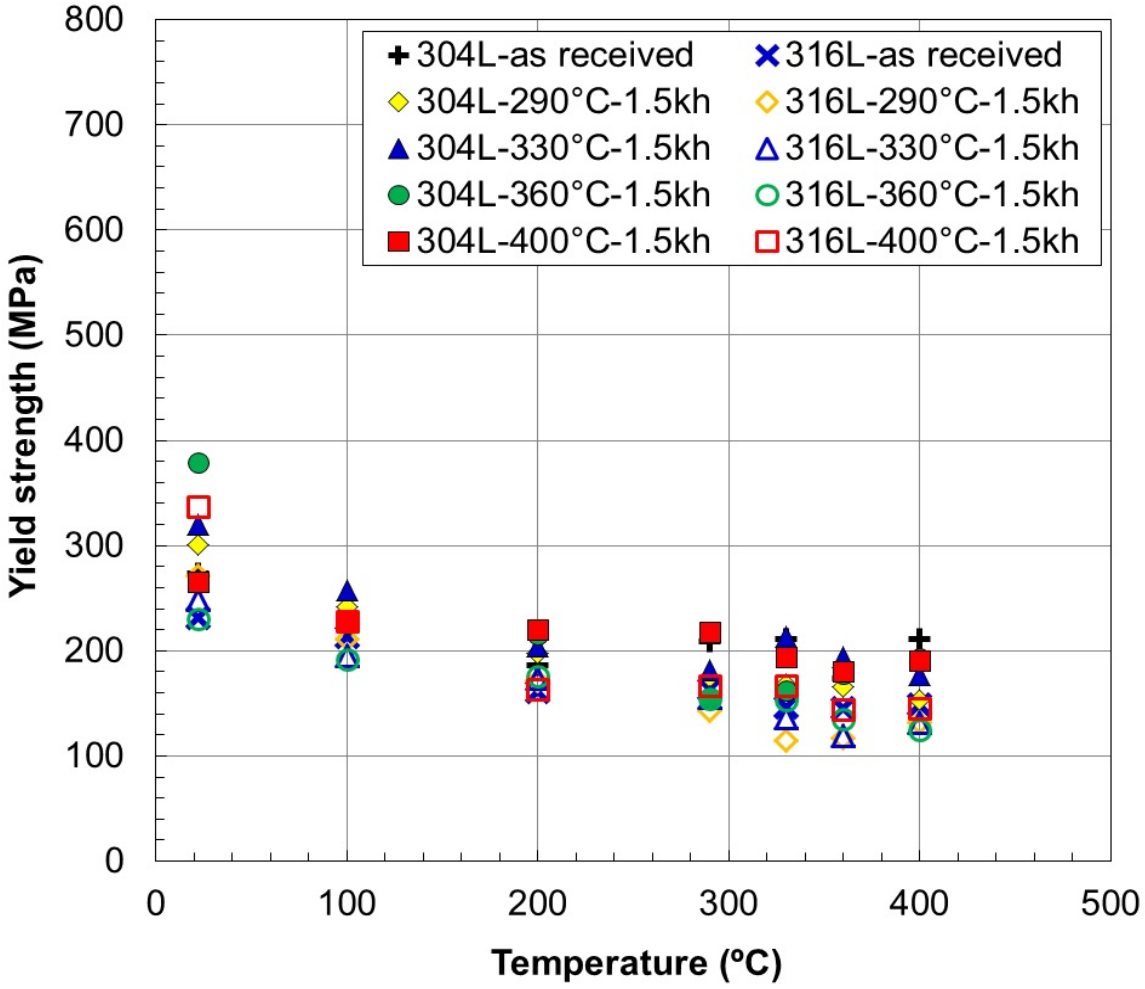

Figure 1. The effect of 1500 hour thermal aging on yield stress (YS) in 304L and 316L austenitic stainless steels.

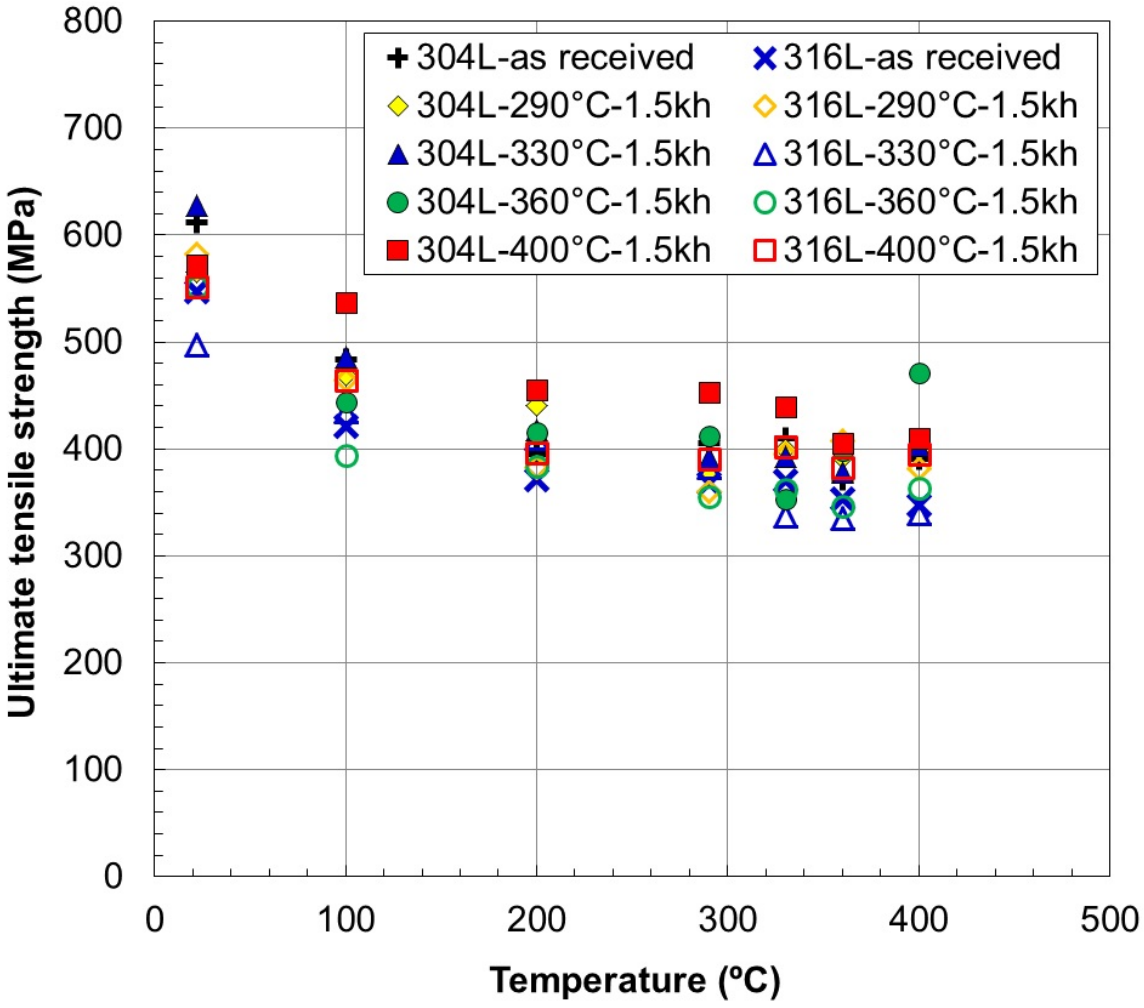

Figure 2. The effect of 1500 hour thermal aging on ultimate tensile strength (UTS) in 304L and 316L austenitic stainless steels.

3.2. Thermal aging effect on ductility

The uniform elongation and total elongation (UE and TE, respectively) for the aged and non-aged austenitic alloys are presented in Figures 3 and 4. Overall, the test temperature dependence of both elongations are similar to those of strength data: the uniform and total elongations after and before the 1500 hour aging decrease with test temperature before they become nearly temperature-independent in the aging temperature region of 290–400 °C. Among the UE datasets the 304L and 316L alloys in as-received condition tend to show relatively steeper decreases with test temperature compared to the aged alloys. This observation, however, cannot be generalized for the TE data as the data scattering is too large. The spreads of UE and TE data are as large as 30% at RT and about 20% in the aging temperature range; these large spreads might indicate that the ductility variation at a temperature are not consistent but just a statistical behavior. Within the aging temperature range, in particular, the data scattering in elongation data seems to be too large

and random to discern any aging-temperature dependent behavior from the noisy variations.

A few general conclusions can be drawn from the strength and ductility data discussed above: The shortest-term aging at 290–400 °C can cause little effect on the tensile property and deformation of the fully austenitic alloys. The strength and ductility data at any temperature distribute within significant bands although the percent variations in the ductility data are larger than those of the strength data.

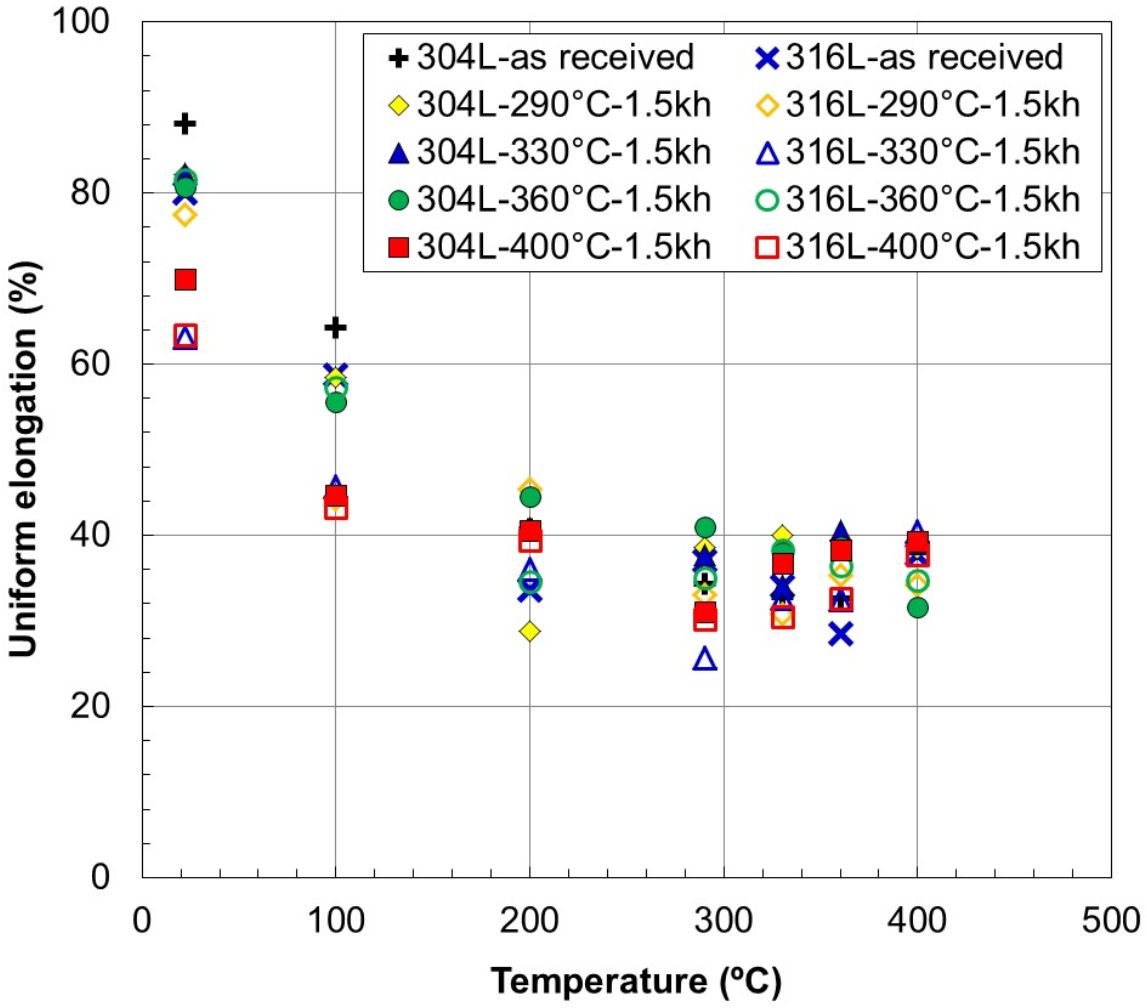

Figure 3. The effect of 1500 hour thermal aging on uniform elongation (UE) in 304L and 316L austenitic stainless steels

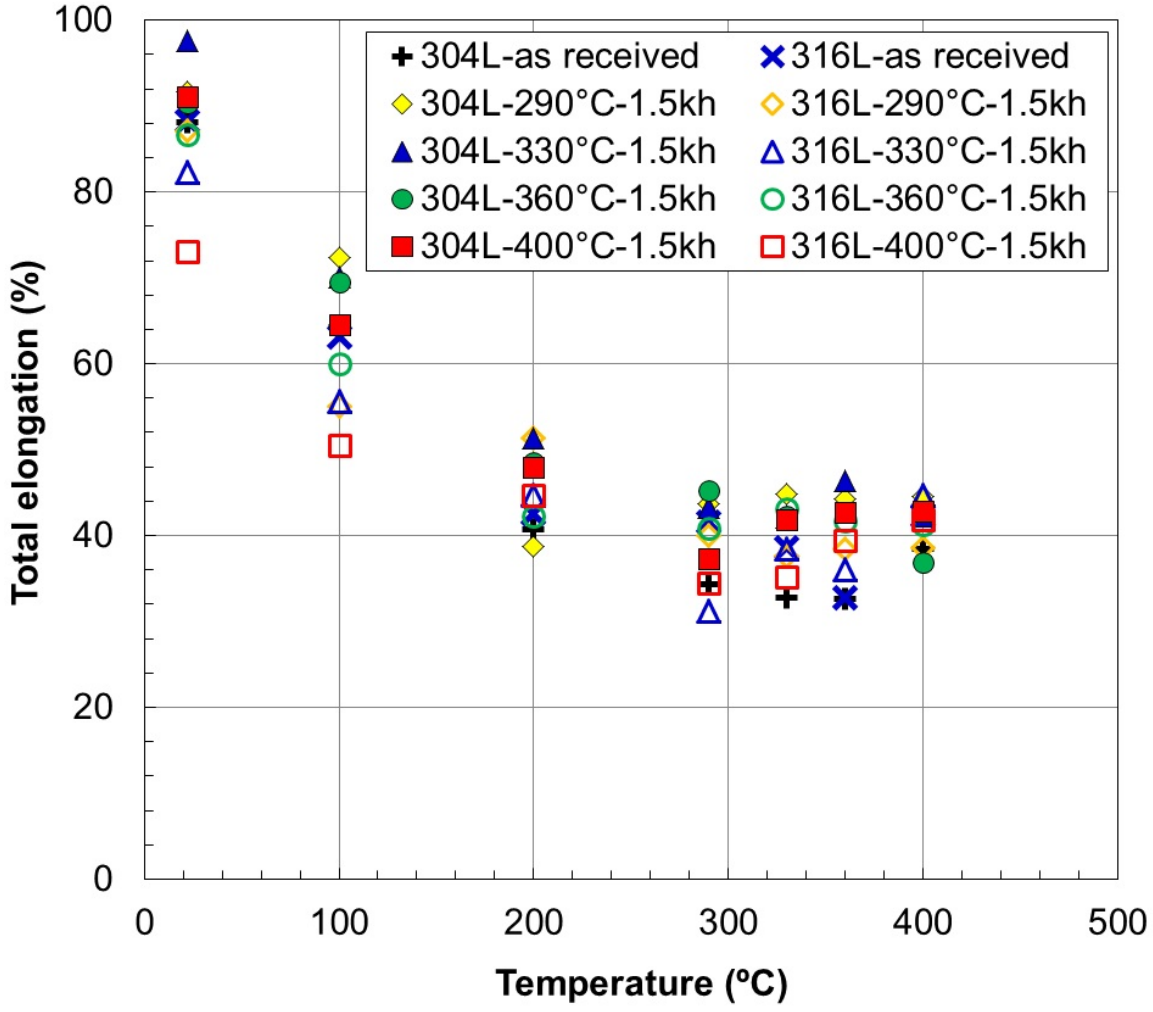

Figure 4. The effect of 1500 hour thermal aging on total elongation (TE) in 304L and 316L austenitic stainless steels

4. IMPACT ENERGY AFTER 1500 H AGING

4.1. Temperature-transition behavior

The absorbed energy datasets obtained in aged and non-aged conditions are presented in Figure 5 for the 304L stainless steel and in Figure 6 for 316L stainless steel. These impact energy data demonstrate that the highly ductile and single phase alloys have excellent impact property over the whole range of aging conditions without showing any noticeable sign of degradation. It is noted that the impact energy plots of non-aged CASS alloys do not have their lower shelves as the measured absorbed energies measured at the lowest test temperature (or in liquid nitrogen) were much higher than the expected lower shelf value of 20 J. These plots also show that only the upper temperature portions of the ductile-brittle transition temperature regions can be present above the liquid nitrogen temperature, i.e., the lowest test temperature. Although the ductile-

brittle transition can be only partially displayed within the practical test temperature range, the temperature transition itself is apparent and such apparent transition should be a unique behavior that can be observed with notched specimens fractured at high speed. These ductile face-centered cubic alloys usually display less apparent ductile-brittle transition in ductility or static fracture toughness versus temperature plots.

It is also commonly observed for the two austenitic alloys in all aging conditions that the impact energy decreases with test temperature above their maximum energy temperatures or upper shelf regions. Interpretation of such decrease with temperature may be a complex task because it is related to the unique deformation characteristics of the low stacking fault alloys showing highly linear dislocation glides. A highly linear glide in austenitic stainless steels usually causes both high strength and high ductility [25]. The impact energy decreasing with test temperature might be caused by simultaneous decrease of strength and ductility as the degree of linear glide is reduced at higher temperatures.

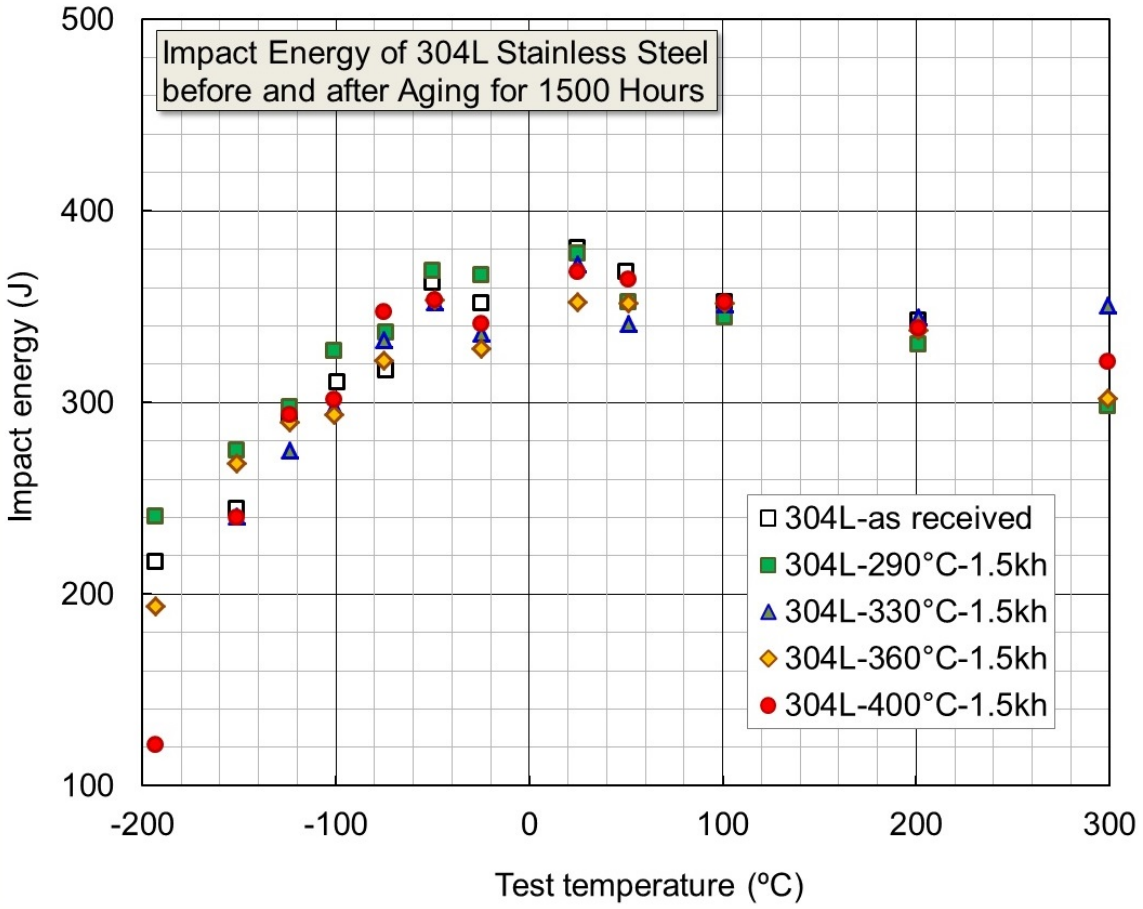

Figure 5. Effect of 1500 hour thermal aging on temperature-transition behavior of Charpy impact energy in 304L austenitic stainless steels.

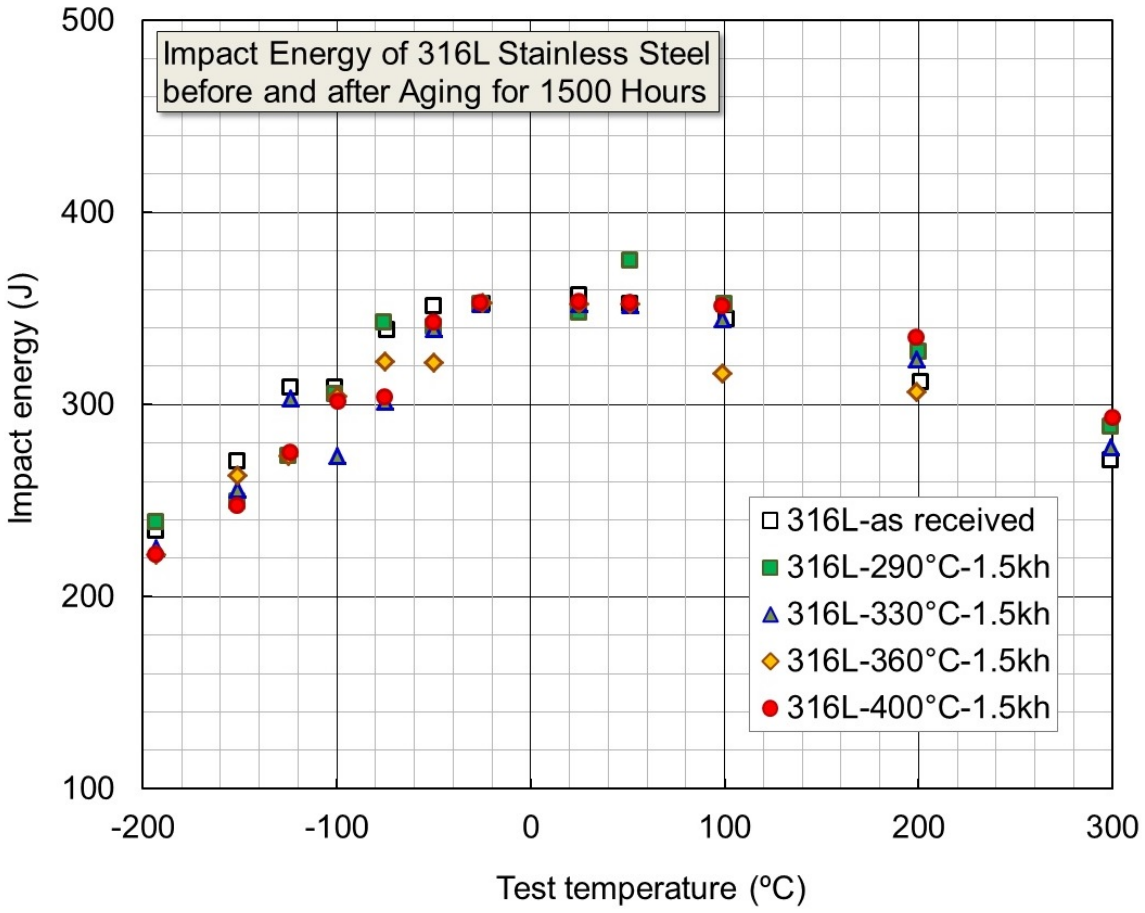

Figure 6. Effect of 1500 hour thermal aging on temperature-transition behavior of Charpy impact energy in 316L austenitic stainless steels.

4.2. Upper shelf energy and ductile-brittle transition temperature

The upper shelf energy and ductile-brittle transition temperature data of aged and non-aged 304L and 316L alloys are presented in Figure 7 and 8, respectively. As displayed in Figures 5 and 6, the vast majority of the measured impact energies were higher than 200 J, and therefore more than half of each complete transition curve could not be drawn. It is therefore noted that the DBTT data calculated by regression analysis are estimated values using the regression functions extrapolated below the liquid nitrogen temperature. The upper shelf energy (USE) was determined as the average of a few highest energy values for each alloy and aging condition.

Figure 7 demonstrates that the 304L and 316L steels can retain USE within a narrow range of 350–375 J regardless of different aging temperatures. There is no clear evidence that the 1500 hour thermal aging has induced any change of USE. Only two cases show meaningful increase or decrease of USE by thermal aging: the 304L alloy after 360 °C aging and the 316L alloy after 290 °C aging. But both of these are seemingly due to experimental scatter.

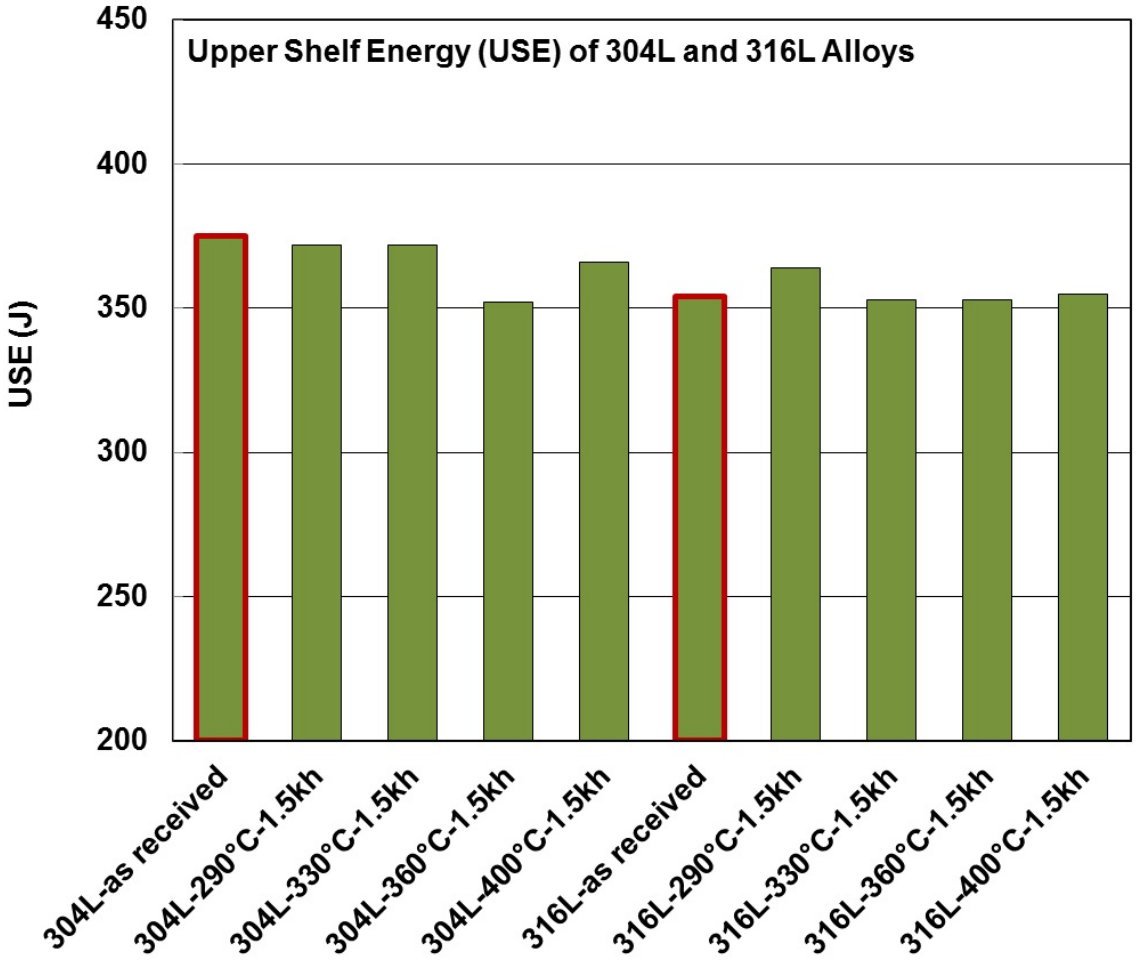

Figure 7. Upper shelf energy of 304L and 316L stainless steels befor and after 1500 hour aging

A similar assessment can be given to the DBTT data of the two test materials: the DBTT data in Figure 8 range from -238 °C to -198 °C or distribute within a 40 °C range. It is confirmed again by this behavior that the 1500 hour thermal aging at 290–400 °C has not degraded the impact property of the fully austenitic steels. It is also noted that none of the DBTTs is above the liquid nitrogen temperature (-196 °C).

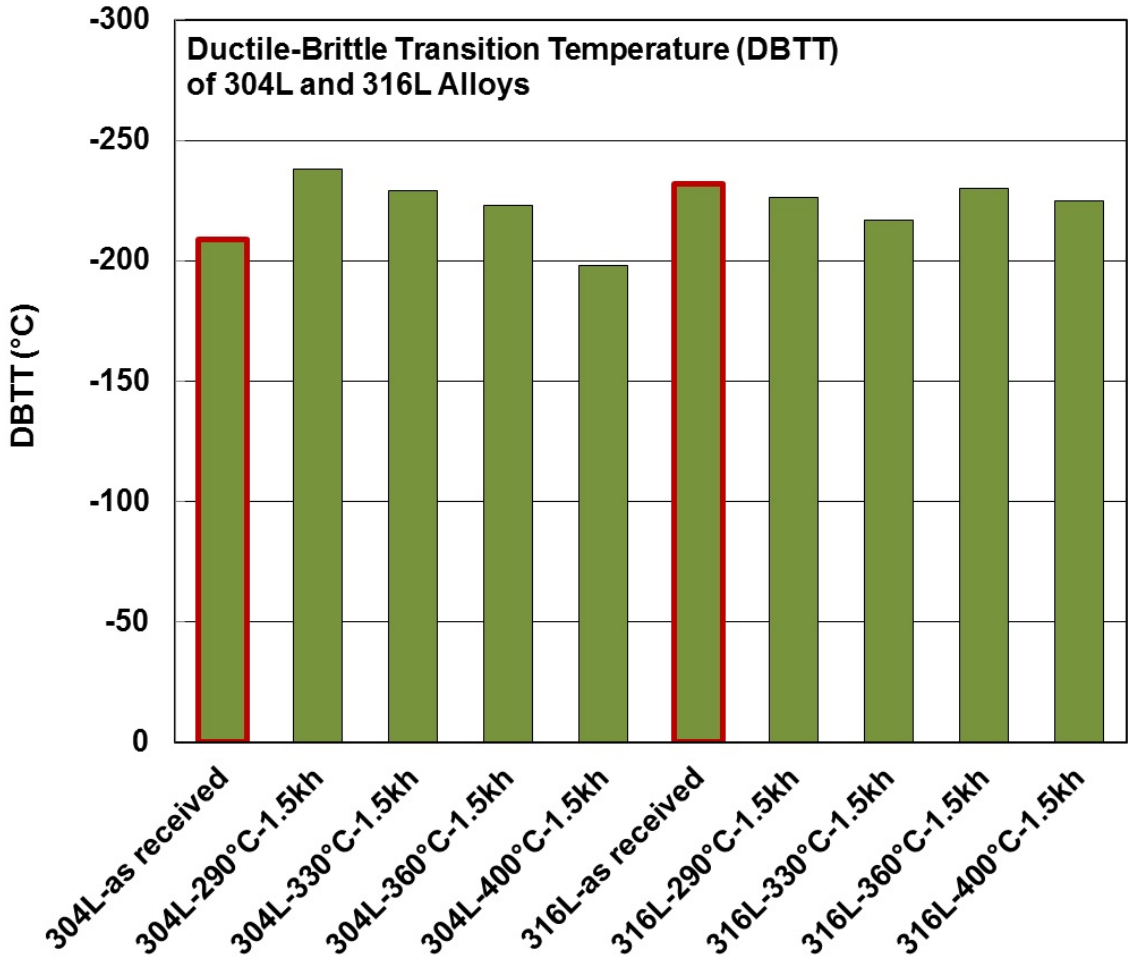

Figure 8. Ductile-brittle transition temperature (DBTT) of 304L and 316L stainless steels befor and after 1500 hour aging

5. CONCLUDING REMARKS

(1) In the Cast Stainless Steel Aging project two purely austenitic 304L and 316L stainless steels have been aged and characterized along with eight cast stainless steels. This report presents the mechanical property test results for the two austenitic alloys after ageing at 290, 330, 360, and 400°C for 1500 hours. The uniaxial tensile and Charpy impact test data in the terms of

various parameters comprise the main datasets discussed in the report, and will be used as reference data to compared with those of cast stainless steels.

(2) The mechanical test data of 304L and 316L stainless steels after 1500 hour aging indicated negligible aging induced degradation: The short-term thermal aging did not cause any significant change in the strength and ductility as well as in the test-temperature dependence of those parameters. The impact energy data demonstrate that the highly ductile and single phase alloys have excellent impact property in all aging conditions without showing any noticeable sign of aging degradation.

(3) There is a sharp contrast between the mechanical behaviors for these purely austenitic (γ) stainless steels and for the cast duplex ($\gamma+\delta$) stainless steels (see M2LW-16OR0402152), which showed significant degradation, in particular, in impact fracture property. The characterization data after 10000 hour aging will be available in the next fiscal year, and it is expected that the aging degradation in these austenitic alloys will become more observable as aging parameter increases. It is also expected that the characterization data of these two purely austenitic alloys after longer-term aging will continue to provide good benchmarking data to discern the degradation component contributed by the δ-ferrite phase from the total aging effect in cast duplex stainless steels.

6. REFERENCES

1. J.T. Busby, P.G. Oberson, C.E. Carpenter, M. Srinivasan, *Expanded Materials Degradation Assessment (EMDA)-Vol. 2: Aging of Core Internals and Piping Systems,* NUREG/CR-7153, Vol. 2, ORNL/TM-2013/532, October 2014.
2. R. Dyle, *Materials Degradation Matrix and Issue Management Tables Overview-LTO Update* (Presented at the Second Workshop on U.S. Nuclear Power Plant Live Extension, Washington, D.C, 2011).
3. T.S. Byun, J.T. Busby, *Cast Stainless Steel Aging Research Plan,* ORNL/LTR-2012/440, September 2012.
4. K. Chopra and A. Sather, *Initial Assessment of the Mechanisms and Significance of Low-Temperature Embrittlement of Cast Stainless Steels in LWR Systems (*NUREG/CR–5385, 1990).
5. Chopra, *Effects of Thermal Aging and Neutron Irradiation on Crack Growth Rate and Fracture Toughness of Cast Stainless Steels and Austenitic Stainless Steel Welds* (NUREG/CR-7185, 2014).
6. K. Chopra, *Estimation of Fracture Toughness of Cast Stainless Steels during Thermal Aging in LWR Systems* (NUREG/CR-4513, 1991).
7. W.F. Michaud, P.T. Toben, W.K. Soppet, and O.K. Chopra, *Tensile-Property Characterization of Thermally Aged Cast Stainless Steels (*NUREG/CR-6142, 1994).
8. H.M. Chung and T R. Leax, *Mater. Sci. Technol.* 6, 249–262 (1990).
9. H.M. Chung, *Evaluation of Aging of Cast Stainless Steel Components* (Presented at ASME

Pressure Vessel & Piping Conference, San Diego, CA, 1991).

10. H. M. Chung, *Presented at the American Society for Mechanical Engineers-Material Properties Council Symposium on Plant Life Extension for Nuclear Components* (Honolulu, Hawaii, 1989).
11. T.S. Byun, Y. Yang, N.R. Overman, J.T. Busby, *Thermal Aging Phenomena in Cast Duplex Stainless Steels,* JOM, 68(2) (2016) 507-526.
12. S. Li, Y.L. Wang, H.L. Zhang, S.X. Li, K. Zheng, F. Xue, X.T. Wang, *J Nucl. Mater.* 433, 41 (2013).
13. M. Murayama, Y. Katayama and K. Hono, *Metall. Mater. Trans. A.* 30A, 345 (1999).
14. T. Sourmail, *Mater. Sci. Tech.* 17, 1 (2001).
15. L.P. Stoter, *J. Mater. Sci.* 16, 1039 (1981).
16. B. Weiss and R. Stickler, *Metal Trans.* 3, 851 (1972).
17. J.E. Spruiell, J.A. Scott, C.S. Ary, and R.L. Hardin, *Metal Trans.* 4, 1533 (1973).
18. J. Charles *Proceedings of Duplex Stainless Steel Conference*, Vol 1 (Les Editions de Physique, Les Ulis Cedex, 1991) pp. 3-48.
19. K.H. Lo, C.H. Shek, J.K.L. Lai, *Mater Sci Eng. R* 65, 39 (2009).
20. P. Hedström, S. Baghsheikhi, P. Liu, J. Odqvist, *Mater. Sci. Eng. A* 534, 552 (2012).
21. C. Pareige, S. Novy, S. Saillet, P. Pareige, *J. Nucl. Mater.* 411, 90 (2011).
22. W. Oldfield, *Curve Fitting Impact Test Data: A Statistical Procedure, ASTM Standardization News,* 3(1 1) (1975) 24-29.
23. K. Yeager, *Nonlinear curve fitting and the Charpy impact test: statistical, mathematical, and physical considerations* (https://www.uakron.edu/dotAsset/2116623.pdf).
24. S.K. Kim, Y.S. Kim, *Estimation of Aging Embrittlement of LWR Primary Pressure Boundary Components,* J. Kor. Nucl. Soc. 30(6) (1998) 609-616.
25. T.S. Byun, N. Hashimoto, K. Farrell, Acta Mater. 52 (2004) 3889–3899.

7. APPENDICES

7.1. Grain structure and elemental distribution in non-aged CASS materials

Microstructural characterization of the as-cast samples has been performed utilizing analytical scanning electron microscopy (SEM), analytical scanning transmission electron microscopy (STEM), and atom probe tomography (APT). The ultimate goal of the characterization is to understand the precipitation and segregation behaviors during casting and aging as well as the origin of embrittlement in cast stainless steels. Preliminary STEM-EDS mapping of just the as-cast model alloys shows some potential insights into their embrittlement behavior, particularly for the Mo-rich alloys. Figure A1 below is a show case showing a series of EDS maps for an austenite-ferrite boundary in CF3M. The austenite region is enriched in Ni, and the ferrite is enriched in Cr and Mo. In addition, the grain boundary is largely enriched in Mo and depleted in Fe relative to the surrounding areas. A similar CF8 boundary has the similar enrichment of Ni in austenite and Cr in ferrite, but there is no noticeable depletion of Fe at the boundary. This offers clues as to why the Mo-rich alloys tend to have a higher temperature sensitivity with respect to the upper shelf energy (USE) from the Charpy Impact tests on the 1500 hour aged samples (see M2LW-16OR0402152), due to the diffusion of Mo to or from the phase boundaries. In Figures A1 and A3, some TEM images showing general microstructures and EDS maps with elemental distributions near grain boundaries are assembled for four model alloys (CF3, CF3M, CF8, and CF8M). The same examination is underway for aged CASS alloys.

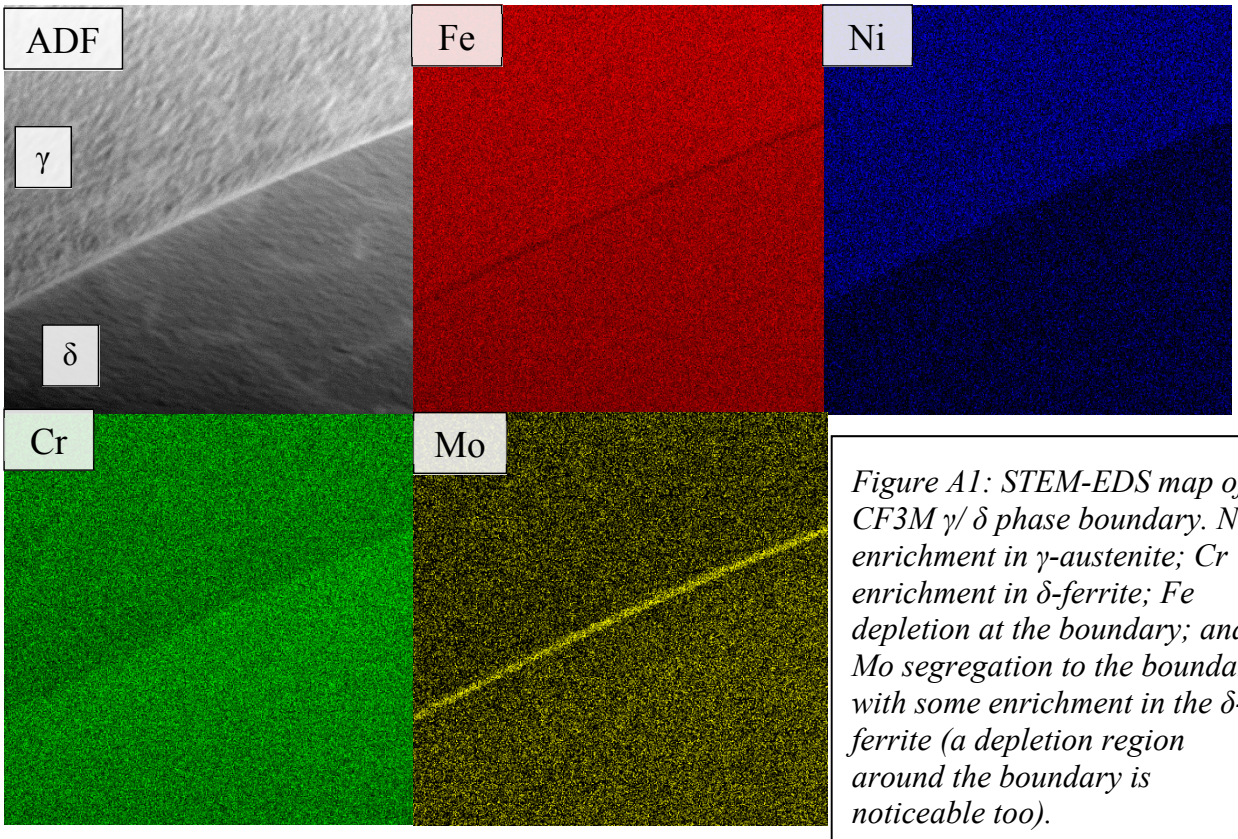

Figure A1: STEM-EDS map of CF3M γ/ δ phase boundary. Ni enrichment in γ-austenite; Cr enrichment in δ-ferrite; Fe depletion at the boundary; and Mo segregation to the boundary with some enrichment in the δ-ferrite (a depletion region around the boundary is noticeable too).

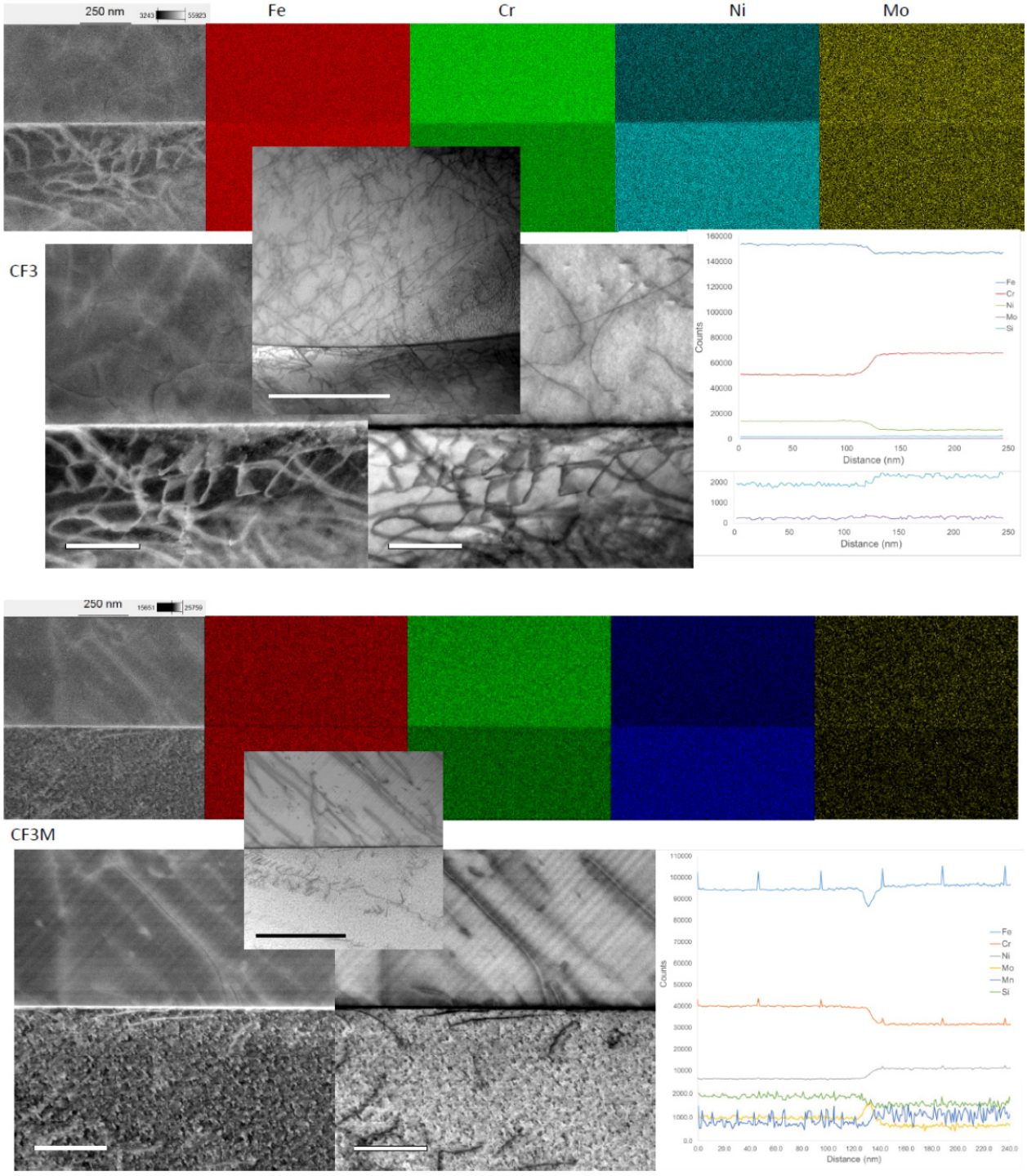

Figure A2: TEM images showing dislocation structures and STEM-EDS map of γ/ δ phase boundary for CF3 (top) and CF3M (bottom) alloys.

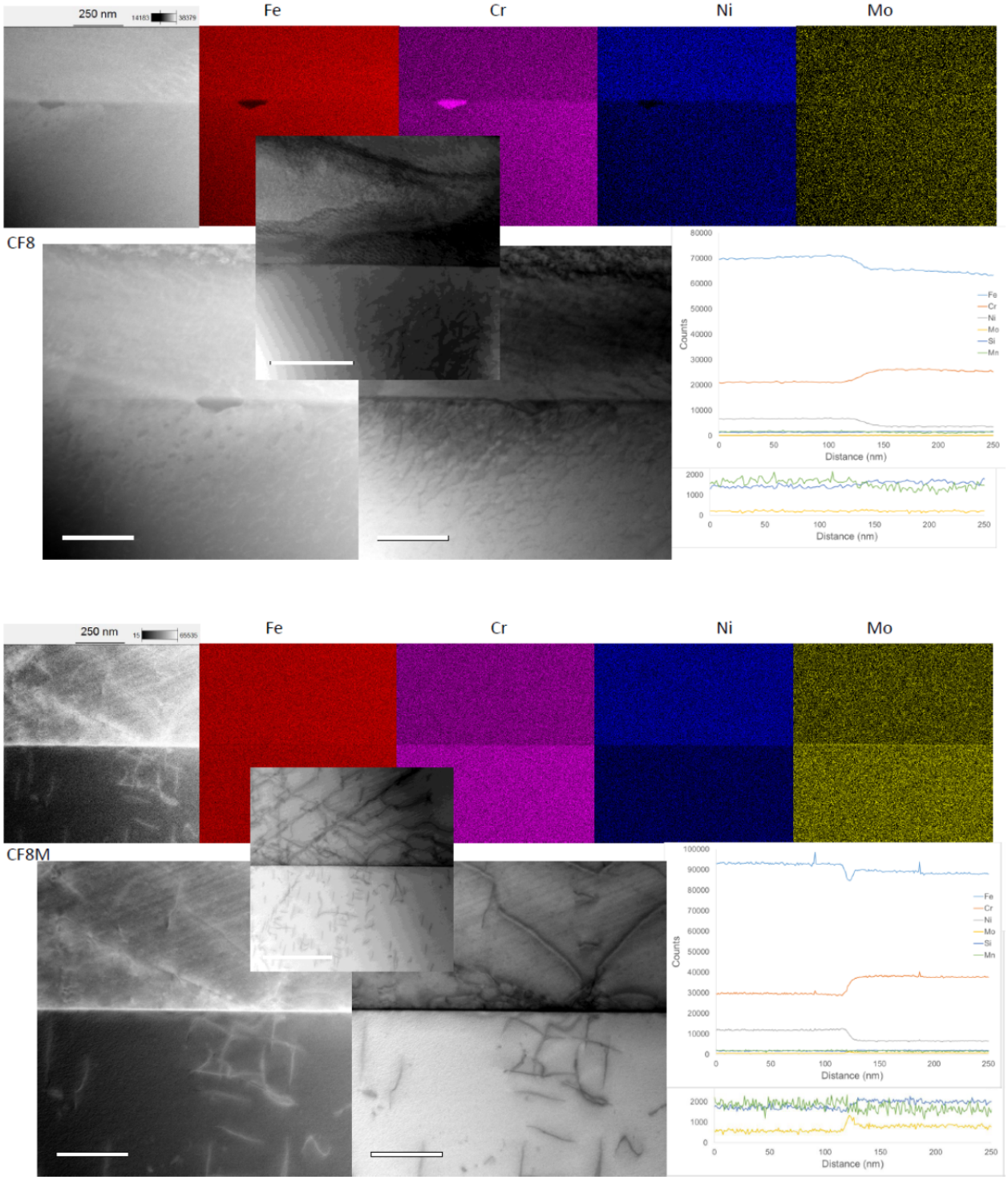

Figure A3: TEM images showing dislocation structures and STEM-EDS map of γ/ δ phase boundary for CF8 (top) and CF8M (bottom) alloys.

EDS line scans and maps have been collected on all four model CASS alloys in the as-cast condition. The line scans in Figure A4 suggest that there is more than just Fe depletion and Mo enrichment at the austenite-ferrite phase boundary in the Mo-heavy alloys (CF3M and CF8M). The Mo-bearing alloys have similar profiles, though the degree of depletion of Fe and enrichment of Mo at the boundary appears to be greater in CF3M. On the other hand, the CF3 and CF8 alloys have much different profiles across the phase boundary; CF3 has the largest difference and CF8 has the smallest difference in Cr and Ni compositions between the austenite and ferrite phases. When compared with the mechanical property data thus far collected, this difference may be a reason for the smaller changes in fracture behavior in the CF8 alloys after thermal aging. The composition and profiles of other elements, such as carbon, will be evaluated with other methods such as EELS and APT to get a thorough evaluation of the as-cast condition. Characterization by STEM-EDS/EELS and APT of the 1500 and 10000 hour aged model alloys at temperatures of 330°C and 400°C is currently underway.

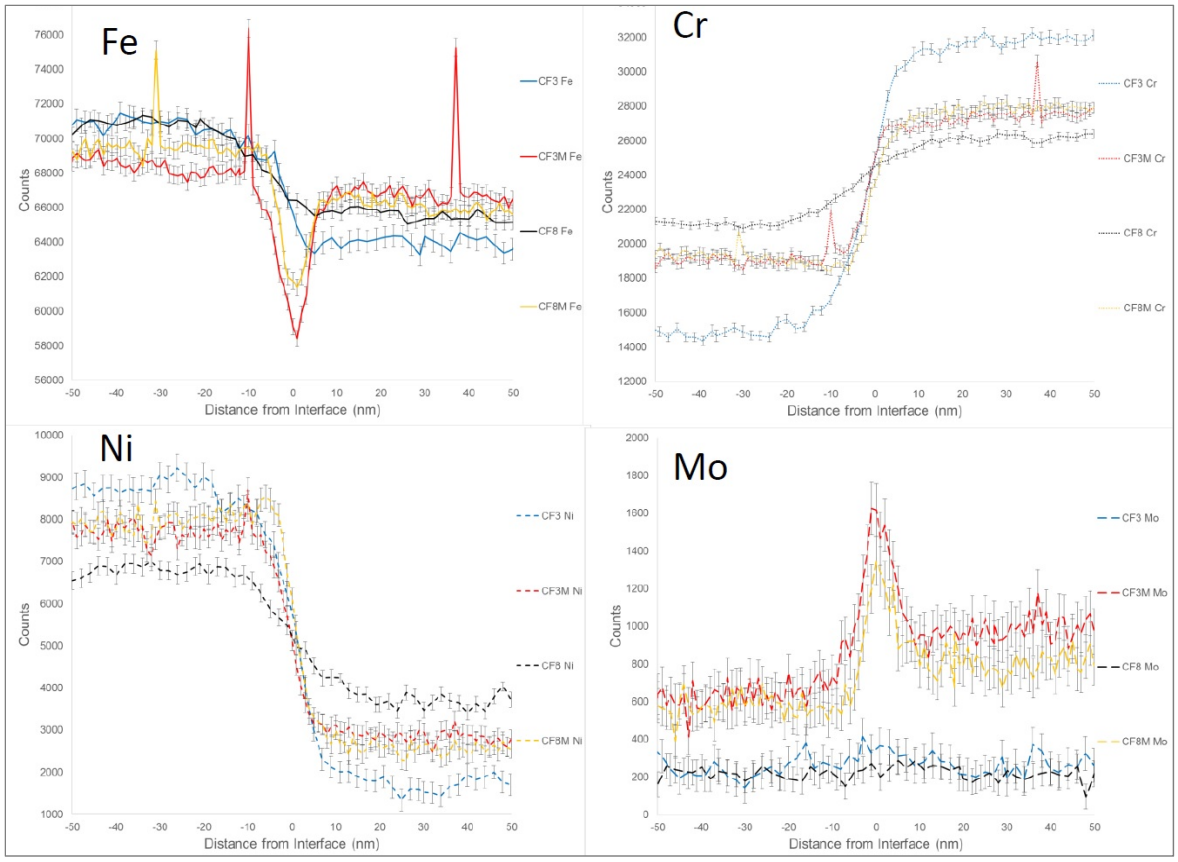

Figure A4: EDS line scans for four primary elements across the ferrite-austenite phase boundary in four as-cast model CASS alloys. Blue-CF3, red-CF3M, black-CF8, yellow-CF8M. These data are all counts that have been adjusted to put elements together for comparison of the relative shapes of data. Absolute count values include errors.

7.2. Progresses in aging and characterization

*Table A1: Status of aging & characterization (**black**-complete/**green**-ongoing/**blue**-planned)*

Source	Alloys	Aging Treatment	Chemistry	Uniaxial Tension	Charpy Impact	Fracture (J-R)	SEM/EBSD	TEM EDX (& APT)
Model	CF3	1500 h 10000 h 30000 h	Baseline (10000 h)	Baseline 1500 h 10000 h (30000 h)	Baseline 1500 h 10000 h (30000 h)	Baseline 1500 h 10000 h (30000 h)	Baseline (10000 h)	Baseline 1500 h 10000 h (30000 h)
Model	CF3M	1500 h 10000 h 30000 h	Baseline (10000 h)	Baseline 1500 h 10000 h (30000 h)	Baseline 1500 h 10000 h (30000 h)	Baseline 1500 h 10000 h (30000 h)	Baseline (10000 h)	Baseline 1500 h 10000 h (30000 h)
Model	CF8	1500 h 10000 h 30000 h	Baseline (10000 h)	Baseline 1500 h 10000 h (30000 h)	Baseline 1500 h 10000 h (30000 h)	Baseline 1500 h 10000 h (30000 h)	Baseline (10000 h)	Baseline 1500 h 10000 h (30000 h)
Model	CF8M	1500 h 10000 h 30000 h	Baseline (10000 h)	Baseline 1500 h 10000 h (30000 h)	Baseline 10000 h (30000 h)	Baseline 1500 h 10000 h (30000 h)	Baseline (10000 h)	Baseline 1500 h 10000 h (30000 h)
EPRI	CF3 (ring)	10000 h 30000 h	Baseline (10000 h)	Baseline 10000 h (30000 h)	Baseline 10000 h (30000 h)	Baseline 10000 h (30000 h)	Baseline (10000 h)	(Baseline) (10000 h)
EPRI	CF8 (ring)	10000 h 30000 h	Baseline (10000 h)	Baseline 10000 h (30000 h)	Baseline 10000 h (30000 h)	Baseline 10000 h (30000 h)	Baseline (10000 h)	(Baseline) (10000 h)
EPRI	CF8 (elbow)	10000 h 30000 h	Baseline (10000 h)	Baseline 10000 h (30000 h)	Baseline 10000 h (30000 h)	Baseline 10000 h (30000 h)	Baseline (10000 h)	(Baseline) (10000 h)
EPRI	CF8M (ring)	10000 h 30000 h	Baseline (10000 h)	Baseline 10000 h (30000 h)	Baseline 1500 h 10000 h (30000 h)	Baseline 10000 h (30000 h)	Baseline (10000 h)	(Baseline) (10000 h)
Reference	304L	1500 h 10000 h 30000 h	*Baseline* (10000 h)	Baseline 1500 h 10000 h (30000 h)	Baseline 1500 h 10000 h (30000 h)	Baseline 1500 h 10000 h (30000 h)	(Baseline) (10000 h)	(Baseline) (10000 h)
Reference	316L	1500 h 10000 h 30000 h	*Baseline* (10000 h)	Baseline 1500 h 10000 h (30000 h)	Baseline 1500 h 10000 h (30000 h)	Baseline 1500 h 10000 h (30000 h)	(Baseline) (10000 h)	(Baseline) (10000 h)

Table A1 summarizes the status of work items performed in the project. The current focus in characterization is on the samples after 10000 hour aging although the fracture toughness testing and TEM/EDX microscopy are performed at relatively slower paces. Below are additional explanations on the status of individual tasks:

- In aging treatment the 1500 hour aging and 10000 hour aging have been completed for all ten portfolio materials.
- Fracture toughness (J-R) tests have been postponed to accumulate more pre-cracked specimens. Precracking for the materials (in green) will be completed first and the J-R testing for those will be carried out as one package.

- Microscopy on reference and EPRI alloys will be selective. Both examination on aged microstructure and fracture mechanism study will be focused on the model alloys.
- The planned test & examination for the 30000 hour aged materials may be subjected to change depending on earlier progress and outcome.
- The work scope of I-NERI collaboration for weld metals is not included in the Table A1. Aging for the weld materials will achieve 10000 hours in FY 2017 and characterization will be started in the same FY following the work items described in the proposal of the I-NERI project.